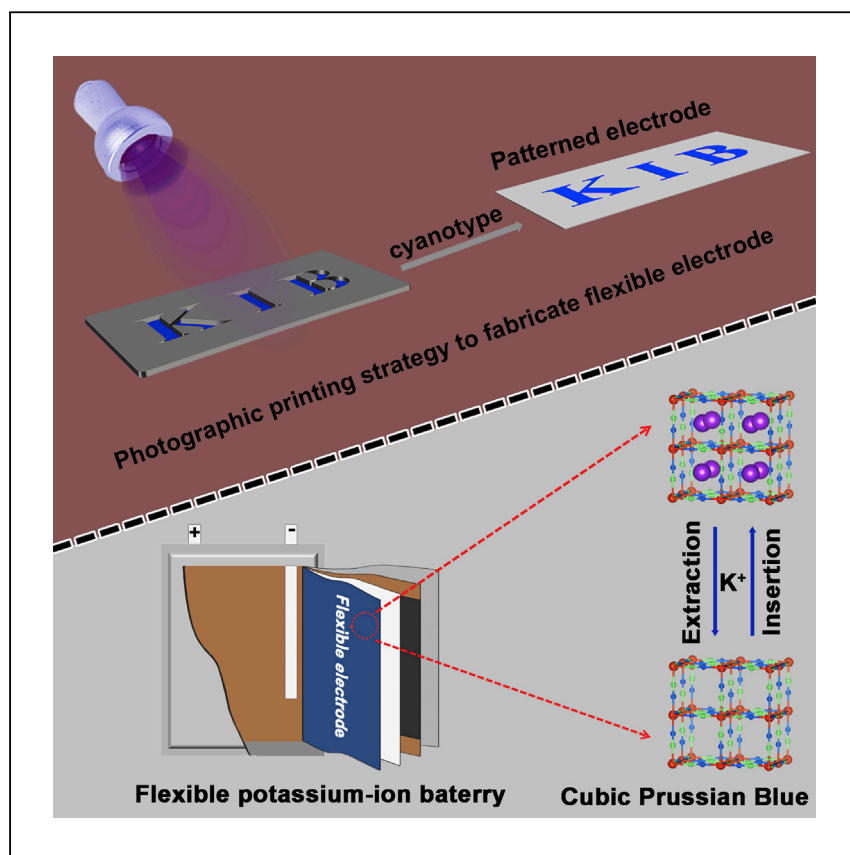


Article

High-Energy-Density Flexible Potassium-Ion Battery Based on Patterned Electrodes



Inspired by traditional cyanotype, we first design a novel strategy for the fabrication of low-cost, lightweight, and soft patterned electrodes. When employed in flexible potassium-ion battery, the patterned electrodes show superior electrochemical performance, including good cycling stability and high energy density. This appealing photographic printing technique as well as the promising electrochemical results opens a new avenue for the fabrication of flexible energy storage systems.

Yun-Hai Zhu, Xu Yang, Di Bao, ..., Xin-Bo Zhang, Jun-Min Yan, Qing Jiang

junminyan@jlu.edu.cn (J.-M.Y.)
jiangq@jlu.edu.cn (Q.J.)

HIGHLIGHTS

Develop a cheap, simple and controllable way to synthesize highly crystalline PB

Build a novel photographic printing strategy to fabricate patterned electrode

Design a flexible potassium-ion battery based on the patterned electrode

Zhu et al., *Joule* 2, 736–746
April 18, 2018 © 2018 Elsevier Inc.
<https://doi.org/10.1016/j.joule.2018.01.010>



Article

High-Energy-Density Flexible Potassium-Ion Battery Based on Patterned Electrodes

Yun-Hai Zhu,¹ Xu Yang,² Di Bao,² Xiao-Fei Bie,³ Tao Sun,² Sai Wang,¹ Yin-Shan Jiang,¹ Xin-Bo Zhang,² Jun-Min Yan,^{1,4,*} and Qing Jiang^{1,*}

SUMMARY

With the rapid development of flexible electronics, low-cost, flexible, high-energy-density power sources are urgently needed. Theoretically, the emerging rechargeable potassium-ion batteries (KIBs) could be a promising candidate due to the abundance and low cost of potassium resources. However, owing to the absence of high-performance cathode materials and effective methods to fabricate robust and soft electrodes, producing flexible KIBs remains a daunting challenge. Herein, cyanotype is successfully employed as a photographic printing technique for the fabrication of a low-cost, scalable, and flexible cathode. The combined advantages of optimized crystallinity and morphology of the cathode materials as well as the ultralight and robust nature of the flexible electrode endow the KIB with superior performance including high energy density (up to 232 Wh kg⁻¹) and excellent flexibility. This low-cost and scalable photographic printing technique as well as the promising electrochemical results will promote the development of flexible electronics.

INTRODUCTION

Flexible electronics have received increasing attention recently, owing to their unique properties and broad application in a variety of fields.^{1–3} To realize low-cost and high-performance flexible electronics, numerous burgeoning flexible energy storage devices have rapidly emerged, including flexible lithium-ion batteries (LIBs), sodium-ion batteries (SIBs), lithium-O₂ batteries, and supercapacitors.^{4–7} Theoretically, the emerging potassium-ion batteries (KIBs) are expected to contribute to flexible electronics due to the low cost and abundance of potassium resources and the relatively low redox potential of K metal (–2.92 V versus the standard hydrogen potential electrode).^{8–12} However, this technology is still in its infancy and numerous scientific and technological challenges need to be overcome for the development of conventional KIBs, not to mention flexible ones. First, the repeated insertion and release of K ions with a significantly large radius (0.138 nm) will easily destabilize the common cathode materials applied in LIBs and SIBs, leading to low capacity, poor rate capability, inferior cycling stability, or even complete electrochemical inactivity in KIBs.^{13,14} Second, the conventional electrodes fabricated by the slurry-casting method can barely maintain structural integrity upon repeated mechanical deformation such as bending, rolling, or folding because of the weak adhesion between the active materials and the smooth surface of the metal substrate.¹⁵ Moreover, the metal current collectors are relatively heavy, decreasing the energy density of the whole battery.¹⁵ To date there have been no reports of flexible

Context & Scale

Flexible electronic devices are leading the trend of next-generation electronic products. Theoretically, the emerging rechargeable potassium-ion batteries (KIBs) could be a promising power source to function them due to the abundance and low cost of potassium resources. However, owing to the absence of high-performance cathode materials and effective methods to fabricate robust and soft electrodes, producing flexible KIBs remains a daunting challenge. Here, we employ a novel photographic printing strategy to fabricate flexible Prussian blue (PB) electrodes by the photoinduced synthesis of highly crystalline PB nanocubes grown onto Xuan paper. Based on the flexible PB electrode, highly flexible KIBs with excellent mechanical strength and superior electrochemical performance are successfully achieved. Our study develops a novel photographic printing flexible electrode and would promote the development of flexible energy storage systems.

KIBs, to say nothing of one with low cost and high energy density. Therefore, there is an urgent need to first develop crystal-structurally stable cathode materials and to fabricate mechanically robust, lightweight as well as self-standing flexible electrodes toward flexible KIBs.

Theoretically, due to its rigid open framework with large interstitial space allowing for rapid ion transport,^{16–19} Prussian blue (PB) and its analogs could be a potentially useful cathode material for flexible KIBs. Conventionally, PB has long been obtained by the spontaneous precipitation method (SPPB), wherein aqueous solution of iron salts combines with the solution of potassium ferrocyanide to precipitate blue PB. However, owing to the extreme insolubility of PB, the crystal nucleation and growth during spontaneous precipitation are generally rapid processes, causing poor crystallinity and severe aggregation of PB particles.²⁰ Although PB can be prepared by either the citrate-assisted coprecipitation method or the hydrothermal method,^{21,22} which are favorable for improving the crystallinity and morphology, these methods suffer from some drawbacks, such as the complexity of the process, low yield, or high energy and/or time cost. Additionally, flexible electrodes with low weight and mechanical robustness are key components in achieving high-energy-density flexible KIB. While several different approaches have been reported for the fabrication of flexible electrodes,^{23–25} the synthesis of self-standing PB electrodes via *in situ* generated highly crystalline PB on a flexible substrate is still highly challenging. Therefore, development of a low-cost, friendly, and facile strategy for the fabrication of lightweight, mechanically robust, and self-standing flexible PB electrodes is highly desired.

Herein, inspired by the fact that traditional cyanotype is a cheap, simple, and controllable precipitation process,^{26–28} we propose cyanotype as a novel photographic printing strategy for the fabrication of low-cost, lightweight, and flexible electrodes by the photoinduced synthesis of highly crystalline PB nanocubes (CTPB) grown onto Xuan paper. When the photographic printing flexible PB electrode is employed as a new class of cathode, highly flexible KIBs with excellent mechanical strength and superior electrochemical performance, including good cycling stability and high energy density, are fabricated. Furthermore, the obtained flexible electrodes are shapeable, which is of great importance for the design and development of personalized energy storage devices.²⁹

RESULTS AND DISCUSSION

Figure 1A displays the reaction mechanism and synthesis process of the cyanotype, which is totally different from the traditional spontaneous precipitation method. First, potassium ferricyanide solution is mixed with ferric ammonium citrate to form a clear brown photosensitizer solution (Figure S1A). Subsequently, the photosensitizer solution is directly irradiated with UV light, causing the Fe^{3+} ions in ferric ammonium citrate to be reduced to Fe^{2+} ions. Finally, the few generated Fe^{2+} ions are immediately consumed by excess ferricyanide ions to form the PB framework (CTPB) accompanied by the simultaneous color change to dark green (Figure S1B)^{30–32} (the detailed reaction mechanisms of cyanotype are described in Figure S2). Note that the insufficient supply of Fe^{2+} ions limits the rate of crystal nucleation and growth, thus resulting in improved crystallinity and dispersion of PB particles. For comparison, SPPB have also been synthesized.

Rietveld-refined X-ray diffraction (XRD) is used to identify the crystal structure of the as-prepared CTPB (Figure 1B). The results show that the obtained samples

¹Key Laboratory of Automobile Materials (Jilin University), Ministry of Education, Department of Materials Science and Engineering, Jilin University, Changchun 130022, China

²State Key Laboratory of Rare Earth Resource Utilization, Changchun Institute of Applied Chemistry, Chinese Academy of Sciences, Changchun 130022, China

³Key Laboratory of Physics and Technology for Advanced Batteries (Ministry of Education), State Key Laboratory of Superhard Materials, College of Physics, Jilin University, Changchun 130012, China

⁴Lead Contact

*Correspondence:
junminyan@jlu.edu.cn (J.-M.Y.),
jiangq@jlu.edu.cn (Q.J.)

<https://doi.org/10.1016/j.joule.2018.01.010>

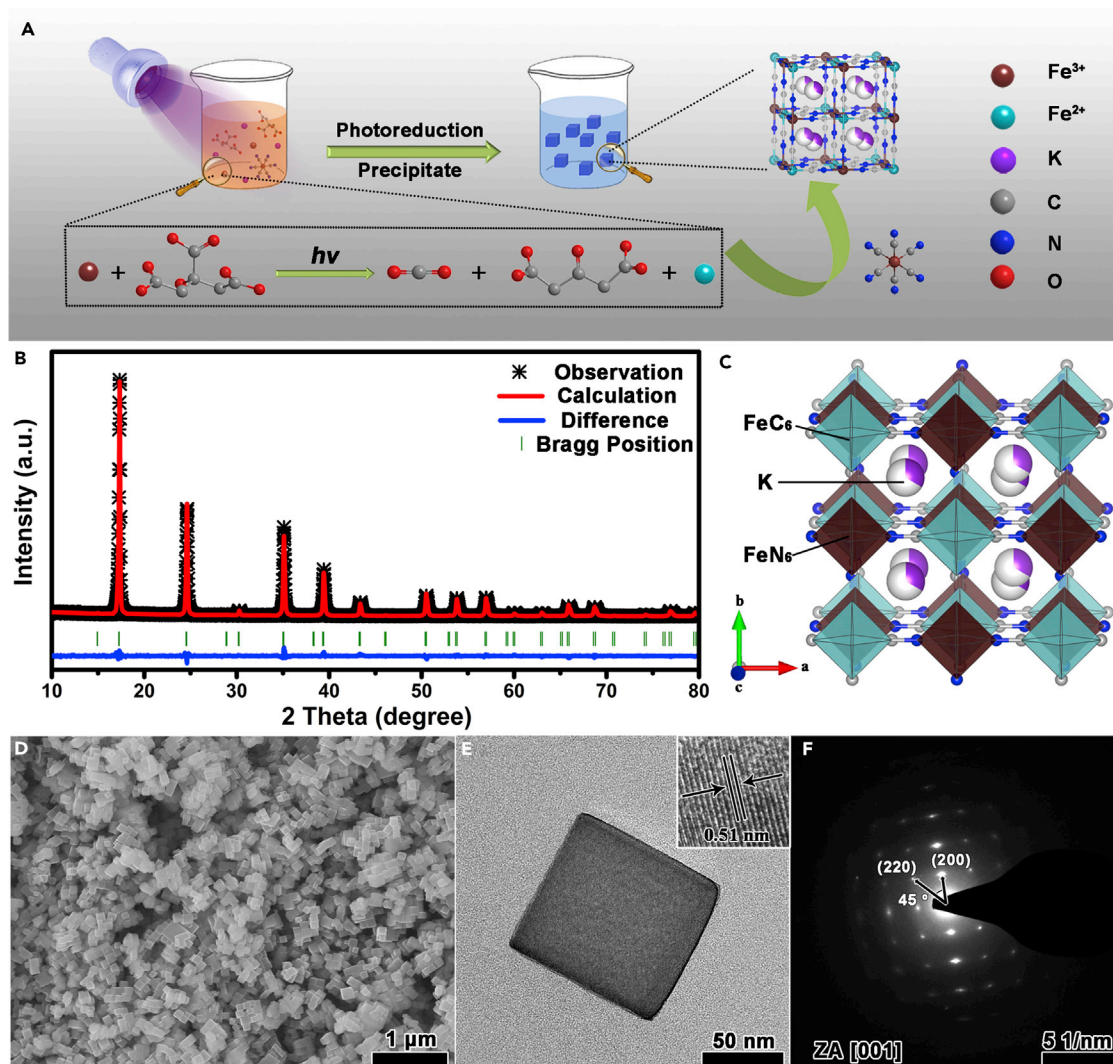


Figure 1. Scheme for Fabrication and Structure of the CTPB

- (A) Schematic illustration of the reaction and formation mechanism of CTPB.
- (B) Rietveld refinement pattern of XRD data for CTPB.
- (C) Schematic representation of the crystal structure of CTPB.
- (D and E) SEM (D) and TEM (E) images of CTPB (inset is the HRTEM image).
- (F) The SAED patterns of a single CTPB particle.

have a cubic symmetry structure with the Fm-3m space group and lattice parameters: $a = b = c = 10.213 \text{ \AA}$ (the detailed refinement results are shown in Table S1). The corresponding refined structural models are also shown in Figures 1C and S3, where two types of iron cation sites forming a double perovskite framework are observed. One iron atom occupies the nitrogen-coordinated sites, forming FeN_6 octahedra, while the other occupies the carbon-coordinated sites, forming FeC_6 octahedra. A 3D framework is formed with the FeC_6 and FeN_6 octahedra bridged by cyanide ligands, providing suitably large diffusion tunnels for the K ions at the interstitial sites. Meanwhile, the crystal structure of SPPB is also examined by XRD, the pattern of which is shown in Figure S4. All diffraction lines of XRD patterns can be indexed as a cubic phase with the Fm-3m space group, in good accordance with the Bragg position calculated from the refined results for CTPB. Note that the

CTPB shows sharp and strong peaks, indicating the highly crystalline nature of CTPB. The X-ray photoelectron spectroscopy results indicate that both CTPB and SPPB contain K, Fe, C, N, and O elements (Figures S5A and S5C). In the Fe 2p spectra (Figures S5B and S5D), the two peaks centered at 707.6 eV and 720.6 eV correspond to the Fe2p3/2 and Fe2p1/2 of Fe²⁺, respectively. The other peaks located at 711.6.7 and 724.8 eV can be attributed to Fe³⁺.³³ To further confirm the chemical composition of the samples, we then employed the inductively coupled plasma-atomic emission spectroscopy method and elemental analysis (Table S2) to determine the mass ratios of the heavy elements (K and Fe) and the light elements (C and N), respectively. When combined with thermogravimetric analysis (TG, Figure S6) to estimate the water content, the chemical formulae of CTPB and SPPB are calculated as K_{0.61}Fe[Fe(CN)₆]_{0.91}·0.32H₂O and K_{0.22}Fe[Fe(CN)₆]_{0.85}·0.64H₂O, respectively.

The morphology and structural characteristics of CTPB and SPPB are further analyzed by scanning electron microscopy (SEM) and transmission electron microscopy (TEM). As shown in Figures 1D and S7, CTPB show a highly regular cubic morphology and high monodispersity. The TEM image (Figure 1E) clearly shows that these monodisperse nanocubes have a uniform diameter of approximately 100 nm. In the high-resolution TEM (HRTEM) images (inset of Figure 1E), the lattice fringe with the d-spacing of 5.10 Å can be observed, which is well matched to the (200) plane of the cubic PB phase. Meanwhile, the corresponding selected-area electron diffraction (SAED) pattern (Figure 1F) indicates the single-crystalline characteristic of the CTPB sample. The set of diffraction spots can be indexed as the (200) and (220) planes along the [001] zone axis. The angle labeled in the SAED pattern is 45°, which is in agreement with the theoretical value of the angle between the (200) and (220) planes. In contrast, SPPB show an irregular morphology and cluttered microsize particles (Figure S8), most likely owing to the aggregation of tiny primary particles during the rapid precipitation process. It is reasonable to assume that the nanoscale electrode materials could provide a short diffusion distance for K ions, favoring a high rate of performance.³⁴

Coin cells with metallic K counter electrodes were assembled, and the galvanostatic discharge/charge technique was employed to evaluate the electrochemical performance of CTPB and SPPB in the voltage window of 2–4.5 V versus K/K⁺. As shown in Figure 2A, the initial charge and discharge capacities of CTPB are 144 and 124 mAh g⁻¹, respectively. The overlapping voltage profiles demonstrate excellent electrochemical reversibility. Apparently, the voltage-capacity profile displays two distinct plateaus; the precise potentials were further analyzed using the differential galvanostatic (dQ/dV) curve (inset of Figure 2A). From the dQ/dV curve, the CTPB electrodes demonstrate two couples of redox peaks at 3.54/3.28 and 4.13/3.95 V versus K/K⁺ attributed to oxidation/reduction of the high-spin configuration Fe²⁺/Fe³⁺ couple (coordinated by N atoms) and the low-spin Fe²⁺/Fe³⁺ configuration (coordinated by C atoms), respectively.³⁵ Figure S9 displays the *ex situ* XRD patterns of CTPB. All of the patterns remain unchanged during the charge-discharge process, indicating K⁺ insertion/extraction via a solid-solution process. Moreover, a shift in the position of the (200) diffraction peak to the bigger angles is observed during charging (Figure S9B), indicating the decrease of the lattice parameter due to the K⁺ extraction. Meanwhile, there is an opposite tendency during discharging, suggesting that CTPB owns excellent structure stability.³⁶ In contrast, the K-ion storage performance of the SPPB electrodes (Figures S10A and S10B) is vastly inferior, with a reversible discharge capacity of only 81 mA hr g⁻¹. Another noteworthy feature of the CTPB electrodes is the rate capability

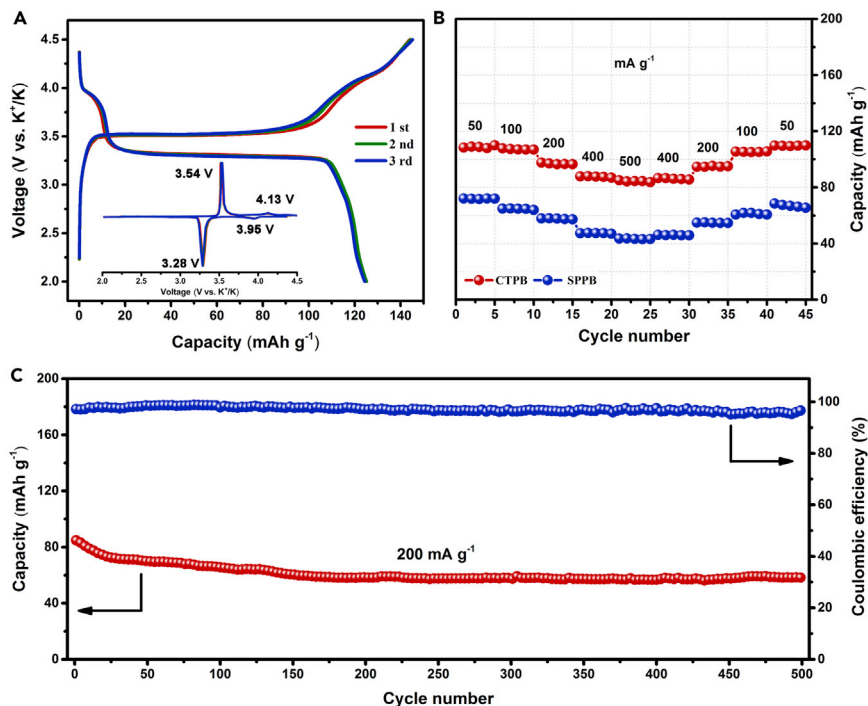


Figure 2. Electrochemical Performance of the CTPB and SPPB

(A) Galvanostatic charge and discharge curves of CTPB at a current density of 10 mA g⁻¹; inset shows the corresponding dQ/dV curves.

(B) Rate capability of CTPB and SPPB at various current densities from 50 to 500 mA g⁻¹.

(C) Cycling performance of CTPB at a current density of 200 mA g⁻¹.

(Figure 2B). As the current densities increase from 50 to 100, 200, 400, and 500 mA g⁻¹, the CTPB electrode delivers good capacity retention, varying from 109 to 107, 97, 88, and 84 mA hr g⁻¹, respectively. Remarkably, when the current density is returned to 50 mA g⁻¹ after 15 cycles, the reversible capacity can be totally recovered to 109 mA hr g⁻¹, corresponding to 100% of its initial reversible capacity. By contrast, the rate performance of the SPPB electrodes is much inferior; less than 93% of the original capacity can be preserved as the current density recovers to 50 mA g⁻¹. Strikingly, the CTPB electrodes also exhibit an excellent cycling stability under high discharge/charge current densities. As shown in Figure 2C, they deliver the higher initial specific capacity of 84.8 mA hr g⁻¹ and maintain the reversible capacity of 58.5 mA hr g⁻¹ after 500 cycles at the current density of 200 mA g⁻¹, corresponding to capacity retentions of 69%. As a comparison, the SPPB electrodes deliver reversible capacities of 36.4 mA hr g⁻¹ after 200 cycles at the same current density (Figure S10C); here only 57% of its initial capacity is preserved. The excellent rate and cycle capability of CTPB is possibly due to its high crystallinity, smaller particle size, and stable crystal structure, as its morphology is without change even after 500 cycles (Figure S11).

Inspired by the advantages of the cyanotype process confirmed above, we then tested its efficacy as a novel strategy for the fabrication of a photographic printing flexible electrode. Figure 3A illustrates the schematic for the formation of a photographic printing pattern electrode. First, a piece of Xuan paper is immersed in the photosensitizer solution to form daylight paper. Subsequently, the obtained daylight paper is assembled together with hollowed-out pattern boards and irradiated with UV light. After developing the UV-treated daylight paper in distilled water

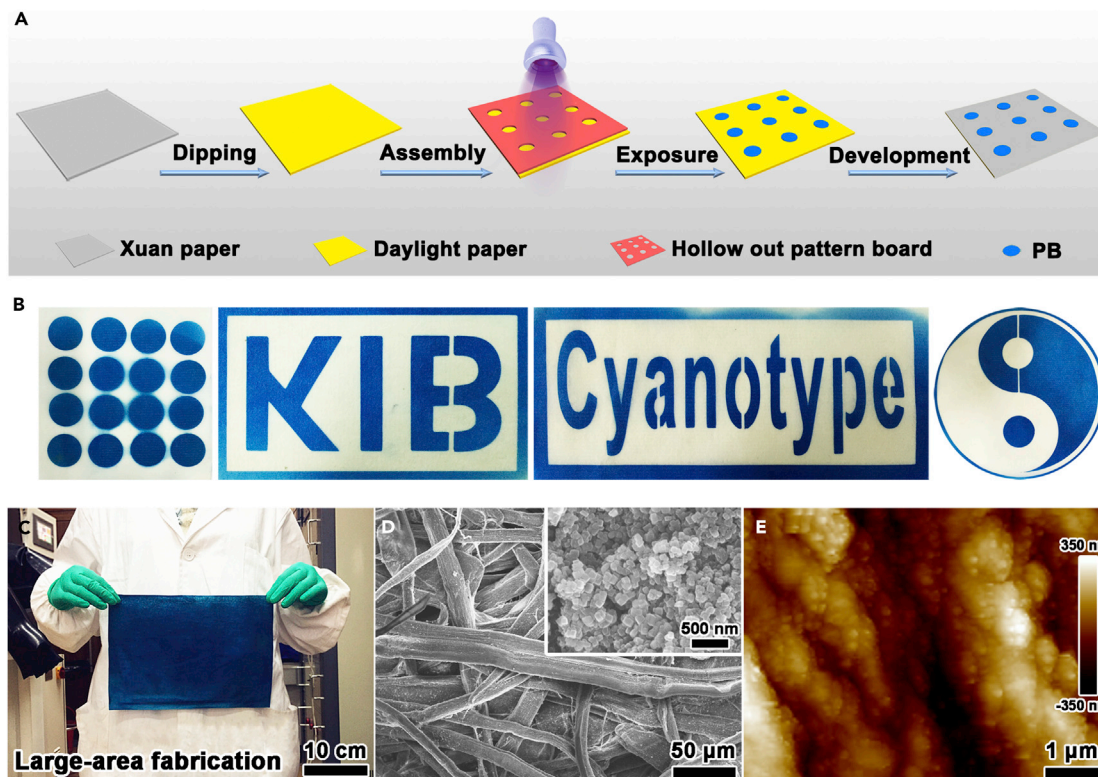


Figure 3. Scheme for Fabrication and Structure of the PP/PB

- (A) Schematic illustration of the formation of PP/PB.
 (B) Photographs of PP/PB with different patterns.
 (C) Fabrication of PP/PB with a large area.
 (D and E) SEM (D) and AFM (E) images of PP/PB (inset is the enlarged SEM image).

and dilute acid solution, the photographic printing PB electrode (PP/PB) can be obtained. Interestingly, the shapes of our electrodes are controllable and depend on the shapes of the hollowed-out pattern boards. Various photographic printing pattern electrodes are displayed in Figure 3B, and their shapes are consistent with those of the hollowed-out pattern boards (Figure S12). More importantly, such synthetic method for PP/PB is scalable for large area fabrication (Figure 3C). It is reasonable to consider that our photographic printing process would be an appealing printing technique and has enormous potential for applications in flexible electronics devices due to features such as low cost, simple processing, atmospheric processing, and possible scalability of fabrication. To further analyze the morphology and structural characteristics of PP/PB electrodes, we employed SEM and atomic force microscopy (AFM). As shown in Figures 3D, 3E, and S13, the surface of the paper fiber is closely stacked with cube-like particles, which is quite different from the smooth surface of the Xuan paper (Figure S14). Meanwhile, the characteristic XRD peaks of the PP/PB electrodes match well with those of the CTPB, thus suggesting the successful formation of PB on the Xuan paper (Figure S15).

Unfortunately, owing to the insulative nature of Xuan paper, the PP/PB electrodes cannot be directly applied in batteries. Consequently, conductive inks (whose major component is Super P) are sprayed on the PP/PB electrodes to form a conductive layer on its surface (PP/PB/SP). Figure 4A shows a photographic image of the

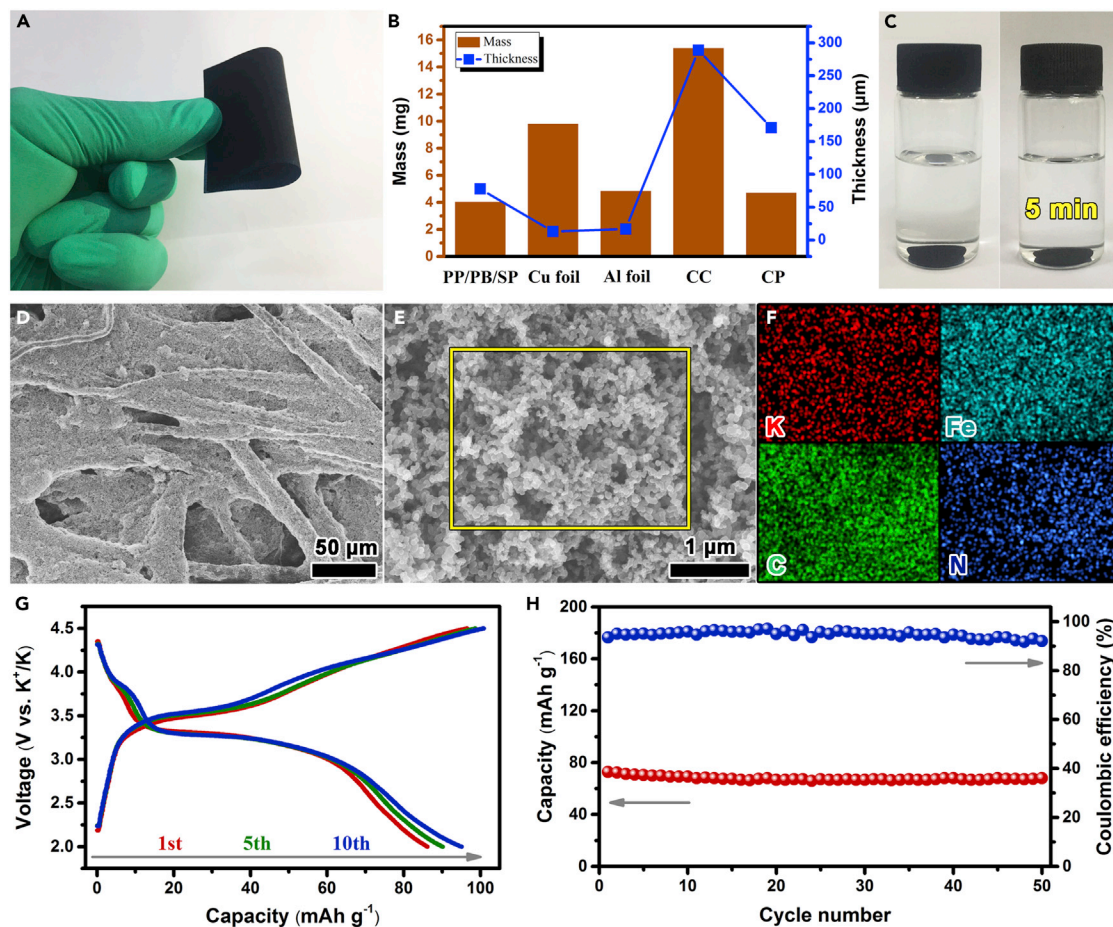


Figure 4. Structure and Electrochemical Performance of the PP/PB/SP

(A) Photograph of the PP/PB/SP in a bending state.

(B) Mass and thickness of PP/PB/SP and other current collector disks.

(C) Photographs of the PP/PB/SP before and after sonication for 5 min in electrolyte.

(D and E) SEM (D) and enlarged SEM (E) images of PP/PB/SP.

(F) EDS mapping images of K, Fe, C, and N in the selected area of (E).

(G and H) Galvanostatic charge and discharge curves (G) and cycle performance (H) of PP/PB/SP at current densities of 50 mA g⁻¹ and 100 mA g⁻¹, respectively.

obtained PP/PB/SP electrodes, exhibiting excellent flexibility and enabling its use for flexible device applications. Since the current collector accounts for ca. 10% of the total weight of the battery, lightweight electrodes will help increase the specific energy density of next-generation energy storage devices.³⁷ Fortunately, the weight of our PP/PB/SP electrode disk (with a diameter of 12 mm) is as low as ca. 4 mg (Figure 4B), even less than that of the common current collector disk (with a diameter of 12 mm), including Cu foil, Al foil, carbon clothes, and carbon paper, although the thickness of PP/PB/SP electrodes is higher than that of Cu foil and Al foil. More importantly, the PP/PB/SP electrodes are mechanically robust. As shown in Figure 4C, the electrolyte remains clear even after being subjected to strong ultrasound for 5 min, indicating that no PB or SP are removed from the electrode into electrolyte. Figures 4D and 4E show the morphology of the PP/PB/SP electrode. After spraying with conductive ink, a 3D porous conductive layer on the surface of PP/PB is constructed. This conductive layer may not only offer an electron transport pathway for active materials but could also enable fast electrolyte mobility.

Corresponding energy-dispersive X-ray spectrometry (EDX) elemental mapping (Figure 4F) reveals that K, Fe, C, and N atoms are homogeneously distributed throughout the electrode, indicating that PP/PB/SP electrodes have been synthesized well.

From the viewpoint of application, we then tested the PP/PB/SP as the integrated electrode in KIBs. As shown in Figure 4G, the voltage-capacity profile of PP/PB/SP displays two distinct plateaus, located ca. 3.3 and 3.9 V on discharge, which is similar to that of CTPB, implying that the K-storage behaviors of PP/PB/SP electrode are the same as those of CTPB. The initial discharge capacity of the PP/PB/SP electrode is 86 mAh g^{-1} . Interestingly, the discharge-voltage plateau located ca. 3.9 V becomes gradually evident over the first ten cycles, thus resulting in the increase of the capacity. After ten cycles the capacity reaches a high level of 95 mAh g^{-1} , indicating the activation of the electrode.³⁸ Figure 4H shows the cycle performance of PP/PB/SP electrode at the current density of 100 mA g^{-1} . It delivers the initial specific capacity of $72.8 \text{ mA hr g}^{-1}$ and maintains the reversible capacity of $68.0 \text{ mA hr g}^{-1}$ after 50 cycles, corresponding to capacity retention of 93.4%. Such excellent cycling ability indicates that our PP/PB/SP electrodes are robust enough to withstand repeated K-ion insertion/extraction.

To demonstrate the application of PP/PB/SP electrodes in flexible electronics, we fabricated flexible KIBs. The structure of the flexible battery is shown in Figures 5A and S16; the battery is composed of the PP/PB/SP cathode, flexible separator, graphite/Cu foil anode, and Al-plastic film. Note that the graphite/Cu foil anode has been potassiated prior to its application in the battery (Figure S17). Figure 5B displays a photograph of the final packaged flexible KIBs, which is consistent with the schematic in Figure 5A. An inset image shown in Figure 5B reveals the excellent flexibility of the device. Figure 5C presents the K-storage performance of the as-prepared flexible battery. The initial discharge capacity is ca. 80 mAh g^{-1} . Subsequently, the discharge capacities remain almost unchanged even after 50 cycles, demonstrating the excellent electrochemical stability. Importantly, the energy density of the final flexible device reaches a very high value of up to 232 Wh kg^{-1} , higher than the values of lead-acid and nickel metal-hydride batteries.^{39–41} To further demonstrate its practical applications, the as-fabricated flexible KIB is used to control a commercial red light-emitting diode (LED). Note that the red LED could be easily lit (Figure 5D) even though the battery is intentionally bent (Figure 5E) and folded (Figure 5F). Furthermore, it can be seen that the discharge capacity remains almost unchanged as the flexible battery is intentionally bent and folded (Figure 5G), indicating that the fabricated flexible KIB is electrochemically stable even when affected by external bending strains.

In summary, using the cyanotype process as a low-cost, nontoxic, and facile method, we have synthesized single-crystalline and highly regular PB nanocubes, which exhibit excellent K-storage performance including high capacity, excellent rate ability, and extremely stable cycling performance. Furthermore, as a proof-of-concept application, photographic printing pattern PB electrodes with features of flexibility, ultralight weight, and mechanical robustness have been successfully fabricated for the first time via the cyanotype process. When the obtained electrode is applied as a new class of cathodes, highly flexible KIBs with excellent mechanical strength and superior electrochemical performance, including good cycling stability and high energy density, are fabricated. This appealing photographic printing technique as well as the promising electrochemical results opens

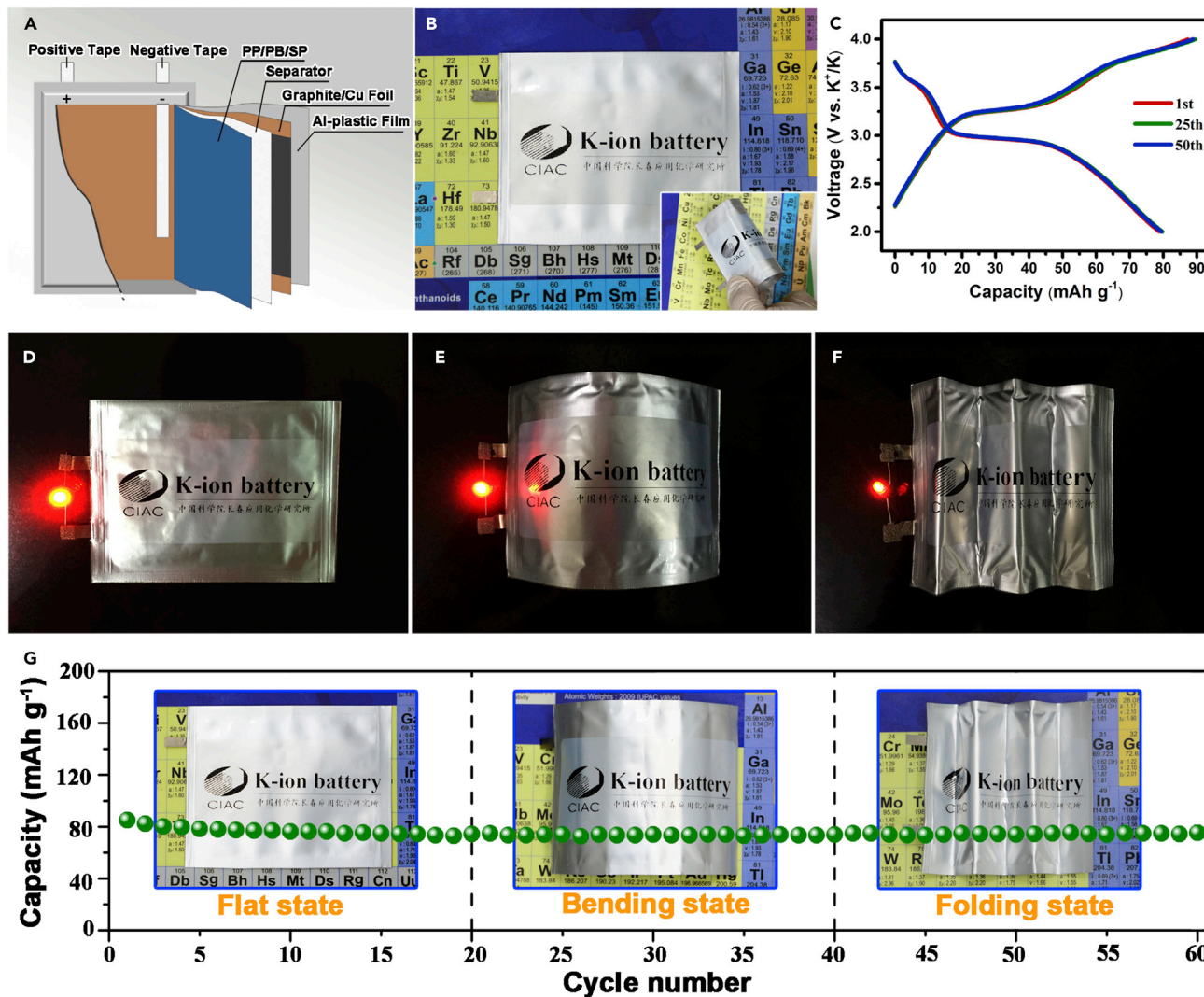


Figure 5. Structure and Bending Properties of Flexible KIBs
 (A) Schematic illustration of the structure of the flexible KIBs.
 (B) Photographs of the fabricated, flexible KIBs.
 (C) Galvanostatic charge and discharge curves of the flexible KIBs at a current density of 50 mA g^{-1} .
 (D–F) Demonstration of an LED light by flexible KIBs under flat (D), bending (E), and folding (F) states.
 (G) Cycle performance of the flexible KIBs under different conditions at a current density of 50 mA g^{-1} .

a new avenue for the fabrication of flexible energy storage systems, which is of great importance for assisting the efforts to design and develop next-generation flexible electronics.

EXPERIMENTAL PROCEDURES

Full experimental procedures are described in [Supplemental Experimental Procedures](#).

SUPPLEMENTAL INFORMATION

Supplemental Information includes Supplemental Experimental Procedures, 17 figures, and 2 tables and can be found with this article online at <https://doi.org/10.1016/j.joule.2018.01.010>.

ACKNOWLEDGMENTS

This work is financially supported by the National Natural Science Foundation of China (51522101, 51631004, and 51471075), Program for JLU Science and Technology Innovative Research Team (2017TD-09), and the Fundamental Research Funds for the Central Universities.

AUTHOR CONTRIBUTIONS

Conceptualization, Y.-H.Z., J.-M.Y., and Q.J.; Methodology, Y.-H.Z., J.-M.Y., and Q.J.; Investigation, Y.-H.Z., X.Y., X.-F.B., T.S., and S.W.; Writing – Original Draft, J.-M.Y., Q.J., and Y.-H.Z.; Writing – Review & Editing, J.-M.Y., Q.J., and Y.-H.Z.; Visualization, Y.-H.Z. and D.B.; Funding Acquisition, X.-B.Z., J.-M.Y., and Q.J.; Resources, Y.-S.J. and X.-B.Z.; Supervision, J.-M.Y., and Q.J.

DECLARATION OF INTERESTS

The authors declare no competing interests.

Received: November 29, 2017

Revised: December 19, 2017

Accepted: January 18, 2018

Published: February 13, 2018

REFERENCES

- Nishide, H., and Oyaizu, K. (2008). Materials science. Toward flexible batteries. *Science* 319, 737–738.
- Wang, X., Lu, X., Liu, B., Chen, D., Tong, Y., and Shen, G. (2014). Flexible energy-storage devices: design consideration and recent progress. *Adv. Mater.* 26, 4763–4782.
- Li, L., Wu, Z., Yuan, S., and Zhang, X.-B. (2014). Advances and challenges for flexible energy storage and conversion devices and systems. *Energy Environ. Sci.* 7, 2101–2122.
- Zhou, G., Li, F., and Cheng, H.-M. (2014). Progress in flexible lithium batteries and future prospects. *Energy Environ. Sci.* 7, 1307–1338.
- Zhu, Y.H., Yuan, S., Bao, D., Yin, Y.B., Zhong, H.X., Zhang, X.B., Yan, J.M., and Jiang, Q. (2017). Decorating waste cloth via industrial wastewater for tube-type flexible and wearable sodium-ion batteries. *Adv. Mater.* 29, 1603719.
- Liu, Q.C., Xu, J.J., Xu, D., and Zhang, X.B. (2015). Flexible lithium-oxygen battery based on a recoverable cathode. *Nat. Commun.* 6, 7892.
- Peng, X., Peng, L., Wu, C., and Xie, Y. (2014). Two dimensional nanomaterials for flexible supercapacitors. *Chem. Soc. Rev.* 43, 3303–3323.
- Eftekhari, A., Jian, Z., and Ji, X. (2017). Potassium secondary batteries. *ACS Appl. Mater. Inter.* 9, 4404–4419.
- Xiao, N., McCulloch, W.D., and Wu, Y. (2017). Reversible dendrite-free potassium plating and stripping electrochemistry for potassium secondary batteries. *J. Am. Chem. Soc.* 139, 9475–9478.
- Ji, B., Zhang, F., Wu, N., and Tang, Y. (2017). A dual-carbon battery based on potassium-ion electrolyte. *Adv. Energy Mater.* 7, 1700920.
- Ji, B., Zhang, F., Song, X., and Tang, Y. (2017). A novel potassium-ion-based dual-ion battery. *Adv. Mater.* 29, 1700519.
- Zuo, W., Zhu, W., Zhao, D., Sun, Y., Li, Y., Liu, J., and Lou, X.W. (2016). Bismuth oxide: a versatile high-capacity electrode material for rechargeable aqueous metal-ion batteries. *Energy Environ. Sci.* 9, 2881–2891.
- Jian, Z., Luo, W., and Ji, X. (2015). Carbon electrodes for K-ion batteries. *J. Am. Chem. Soc.* 137, 11566–11569.
- Zhu, Y.H., Yin, Y.B., Yang, X., Sun, T., Wang, S., Jiang, Y.S., Yan, J.M., and Zhang, X.B. (2017). Transformation of rusty stainless-steel meshes into stable, low-cost, and binder-free cathodes for high-performance potassium-ion batteries. *Angew. Chem. Int. Ed.* 56, 7881–7885.
- Pan, S., Ren, J., Fang, X., and Peng, H. (2016). Integration: an effective strategy to develop multifunctional energy storage devices. *Adv. Energy Mater.* 6, 1501867.
- Wang, L., Song, J., Qiao, R., Wary, L.A., Hossain, M.A., Chuang, Y.D., Yang, W., Lu, Y., Evans, D., Lee, J.J., et al. (2015). Rhombohedral Prussian white as cathode for rechargeable sodium-ion batteries. *J. Am. Chem. Soc.* 137, 2548–2554.
- Eftekhari, A. (2004). Potassium secondary cell based on Prussian blue cathode. *J. Power Source* 126, 221–228.
- Shadiké, Z., Shi, D.R., Cao, M.H., Yang, S.F., Chen, J., and Fu, Z.W. (2017). Long life and high-rate Berlin green FeFe(CN)₆ cathode material for a non-aqueous potassium-ion battery. *J. Mater. Chem. A* 5, 6393–6398.
- Liao, J., Hu, Q., Yu, Y., Wang, H., Tang, Z., Wen, Z., and Chen, C. (2017). A potassium-rich iron hexacyanoferrate/dipotassium terephthalate@carbon nanotube composite used for K-ion full-cells with an optimized electrolyte. *J. Mater. Chem. A* 5, 19017–19024.
- Wessells, C.D., Peddada, S.V., Huggins, R.A., and Cui, Y. (2011). Nickel hexacyanoferrate nanoparticle electrodes for aqueous sodium and potassium ion batteries. *Nano Lett.* 11, 5421–5425.
- He, G., and Nazar, L.F. (2017). Crystallite size control of Prussian white analogues for nonaqueous potassium-ion batteries. *ACS Energy Lett.* 2, 1122–1127.
- Zheng, X.J., Kuang, Q., Xu, T., Jiang, Z.Y., Zhang, S.H., Xie, Z.X., Huang, R.B., and Zheng, L.S. (2007). Growth of Prussian blue microcubes under a hydrothermal condition: possible nonclassical crystallization by a mesoscale self-assembly. *J. Phys. Chem. C* 111, 4499–4502.
- Zhang, W., Liu, Y., Chen, C., Li, Z., Huang, Y., and Hu, X. (2015). Flexible and binder-free electrodes of Sb/rGO and Na₃V₂(PO₄)₃/rGO nanocomposites for sodium-ion batteries. *Small* 11, 3822–3829.
- Liu, Y., Zhang, N., Jiao, L., and Chen, J. (2015). Tin nanodots encapsulated in porous nitrogen-doped carbon nanofibers as a free-standing anode for advanced sodium-ion batteries. *Adv. Mater.* 27, 6702–6707.
- Ding, Y.L., Wu, C., Kopold, P., van Aken, P.A., Maier, J., and Yu, Y. (2015). Graphene-protected 3D Sb-based anodes fabricated via electrostatic assembly and confinement replacement for enhanced lithium and sodium storage. *Small* 11, 6026–6035.

26. Turner, J., Parisi, A.V., Downs, N., and Lynch, M. (2014). From ultraviolet to Prussian blue: a spectral response for the cyanotype process and a safe educational activity to explain UV exposure for all ages. *Photochem. Photobiol. Sci.* 13, 1753–1764.
27. Morizot, O., Audureau, E., Briand, J.Y., Hagel, G., and Boulc'h, F. (2015). Introducing the human element in chemistry by synthesizing blue pigments and creating cyanotypes in a first-year chemistry course. *J. Chem. Educ.* 92, 74–78.
28. Ware, M. (2008). Prussian blue: artists' pigment and chemists' sponge. *J. Chem. Educ.* 85, 612.
29. Yang, X., Zhang, H., Chen, Y., Yu, Y., Li, X., and Zhang, H. (2017). Shapeable electrodes with extensive materials options and ultra-high loadings for energy storage devices. *Nano Energy* 39, 418–428.
30. Abrahamson, H.B., Rezvani, A.B., and Brushmiller, J.G. (1994). Photochemical and spectroscopic studies of complexes of iron (III) with citric acid and other carboxylic acids. *Inorg. Chim. Acta* 226, 117–127.
31. Lawrence, G.D., and Fishelson, S. (1999). UV catalysis, cyanotype photography, and sunscreens. *J. Chem. Educ.* 76, 1199.
32. Abrahamson, H.B. (2001). The photochemical basis of cyanotype photography. *J. Chem. Educ.* 78, 311.
33. Zhang, C., Xu, Y., Zhou, M., Liang, L., Dong, H., Wu, M., Yang, Y., and Lei, Y. (2017). Potassium Prussian blue nanoparticles: a low-cost cathode material for potassium-ion batteries. *Adv. Funct. Mater.* 27, 1604307.
34. Bie, X., Kubota, K., Hosaka, T., Chihara, K., and Komaba, S. (2017). A novel K-ion battery: hexacyanoferrate (II)/graphite cell. *J. Mater. Chem. A* 5, 4325–4330.
35. Wu, X., Jian, Z., Li, Z., and Ji, X. (2017). Prussian white analogues as promising cathode for non-aqueous potassium-ion batteries. *Electrochem. Commun.* 77, 54–57.
36. Chong, S., Chen, Y., Zheng, Y., Tan, Q., Shu, C., Liu, Y., and Guo, Z. (2017). Potassium ferrous ferricyanide nanoparticles as high capacity and ultralong life cathode material for nonaqueous potassium-ion batteries. *J. Mater. Chem. A* 5, 22465–22471.
37. Richa, K., Babbitt, C.W., Gaustad, G., and Wang, X. (2014). A future perspective on lithium-ion battery waste flows from electric vehicles. *Resour. Conserv. Recycl.* 83, 63–76.
38. Huang, X.L., Xu, D., Yuan, S., Ma, D.L., Wang, S., Zheng, H.Y., and Zhang, X.B. (2016). Dendritic Ni-P-coated melamine foam for a lightweight, low-cost, and amphipathic three-dimensional current collector for binder-free electrodes. *Adv. Mater.* 26, 7264–7270.
39. Rydh, C.J. (1999). Environmental assessment of vanadium redox and lead-acid batteries for stationary energy storage. *J. Power Source* 80, 21–29.
40. Gifford, P., Adams, J., Corrigan, D., and Venkatesan, S. (1999). Development of advanced nickel/metal hydride batteries for electric and hybrid vehicles. *J. Power Source* 80, 157–163.
41. Zhang, X., Tang, Y., Zhang, F., and Lee, C.S. (2016). A novel aluminum-graphite dual-ion battery. *Adv. Energy Mater.* 6, 1502588.